Probing the Goldstone equivalence theorem in heavy weak doublet decays

Bhaskar Dutta,[1] Yu Gao,[1] David Sanford,[2] and Joel W. Walker[3]

[1]*George P. and Cynthia W. Mitchell Institute for Fundamental Physics and Astronomy, Texas A&M University, College Station, Texas 77843, USA*

[2]*Walter Burke Institute for Theoretical Physics, California Institute of Technology, Pasadena, California 91125, USA*

[3]*Department of Physics, Sam Houston State University, Huntsville, Texas 77341, USA*

(Received 25 September 2015; published 15 March 2016)

This paper investigates the decays from heavy Higgsino-like weak doublets into Z, h bosons and missing particles. When pair-produced at the LHC, the subsequent Z, $h \to \ell\ell$, $b\bar{b}$ decays in the doublet decay cascade can yield 4ℓ, $2\ell 2b$ and $4b + \not{E}_{\mathrm{T}} + j(\mathrm{s})$ final states. Mutual observation of any two of these channels would provide information on the associated doublets' decay branching fractions into a Z or h, thereby probing the Goldstone equivalence relation, shedding additional light on the Higgs sector of beyond the Standard Model theories and facilitating the discrimination of various contending models, in turn. We compare the Z/h decay ratio expected in the minimal supersymmetric model, the next-to-minimal supersymmetric model (NMSSM)and a minimal singlet-doublet dark matter model. Additionally, we conduct a full Monte Carlo analysis of the prospects for detecting the targeted final states during 14 TeV running of the LHC in the context of a representative NMSSM benchmark model.

DOI: 10.1103/PhysRevD.93.055020

I. INTRODUCTION

The Higgs mechanism plays a central role in the electroweak symmetry breaking, and many beyond the Standard Model (BSM) frameworks have been proposed to generate the correct weak-scale Higgs mass as well as to protect it from the ultraviolet (UV) divergence. In any such spontaneous symmetry breaking scenario, there are massless spin-0 (Goldstone) excitations along flat directions of the potential that realize the underlying symmetry of the Lagrangian. If the symmetry is gauged, these degrees of freedom are absorbed in the longitudinal modes of the newly massive vectors, and the Goldstone equivalence theorem mandates that amplitudes for longitudinal vector bosons will be equivalent to those of the associated Goldstone at large collision energies. In particular, for both the Standard Model (SM) and BSM cases, given that the Z mass arises from the Higgs vacuum expectation value (VEV) v, the Z longitudinal modes and the Higgs boson share common couplings, and a (near) unit ratio of Z/h production is generically expected. While there are no heavy electroweak states in the SM to decay directly to Z and h bosons, new states with a nonzero electroweak charge exist in many BSM theories, and their decay branching fraction into Z and h may be applied as a very useful probe of the Higgs sector in such models.

Supersymmetry (SUSY) has been widely accepted as a viable mechanism for alleviating large UV fermion-loop corrections to the Higgs mass. In R-parity-enforcing SUSY models, the lightest (LSP) and the next-to-lightest supersymmetric particle (NLSP) may be neutralinos. The NLSP may decay into the LSP along with a Z or h. This channel is particularly favorable when there are no other particles in the spectrum, e.g., sfermions, appearing between the lightest two neutralinos that may reduce the branching fraction into Z and h. In the minimal supersymmetric standard model (MSSM), scenarios with a binolike LSP and Higgsino-like NLSPs are quite common, since lighter Higgsinos are preferred in order to realize a smaller value of the SUSY-preserving Higgsino mixing term μ. Moreover, since anomaly cancellation requires distinct $SU(2)_{\mathrm{L}}$ Higgs doublets (H_u, H_d) to provide up- and downlike masses, there are two Higgsino NLSPs in this case. The Z, h decay branching fractions of each depend sensitively on the individual neutralino mixing of H_u, H_d, although the ratio of the decay branching ratios into Z and h is of order unity when both contributions are added, as predicted by the Goldstone equivalence theorem. Nevertheless, the specific ratio may feature some weak residual dependence upon the specific model parameters, particularly the ratio $\tan\beta$ of VEVs acquired by the up and down type MSSM Higgs fields.

It is interesting to consider alternative scenarios that can impact the Z/h branching ratio. For example, testable deviation from the MSSM could be predicted if the Higgs mixes with other fundamental scalars that couple outside of the $SU(2)_{\mathrm{L}}$ gauge structure, such as the singlet field S in the next-to-minimal supersymmetric model (NMSSM) [1–3]. This extension is independently well motivated as a solution to the naturalness problem, providing an explanation for why the μ term might be light, of electroweak order, counterbalancing similarly sized contributions to the Z mass that emerge explicitly from the soft SUSY-breaking sector. Specifically, the μ term arises dynamically in this

context, as the VEV of a new singlet chiral supermultiplet containing a pair of charge-parity (CP) even/odd scalars, as well as a fifth "singlino" neutralino. One or both of the (pseudo)scalars may take masses above or around the 125 GeV scale, and potentially confuse the interpretation of fermion pair mass measurements at colliders. Since S is a singlet, and does not participate in the Higgs mechanism, its mixing into the observed Higgs scalar can reduce the Higgs coupling to the doublet NLSPs. Similarly, if a singlet pseudoscalar around 125 GeV emerges in decays, it can significantly suppress the observed branching fraction into Z by enhancing the observed Higgs-like fraction.

An alternative, explicitly nonsupersymmetric, spectral modification that we will entertain for the sake of comparison and contrast involves extension of the SM using singlet-doublet fermionic (SDF) dark matter [4]. This type of model introduces a singlet fermion S that couples to the SM Higgs field via two heavier doublets D_1, D_2, allowing for cascade decays into the same final states as the previously described NMSSM scenario. However this scenario can potentially be distinguished from the NMSSM by measuring the Z/h ratio, since the new fermions do not alter the Higgs sector or modify the Higgs mass.

At the LHC, the counts of $b\bar{b}$ and opposite-sign (OS) like-flavor (LF) light lepton pairs that reconstruct h or Z masses in a $2Z/h + \not{E}_{\mathrm{T}} + \mathrm{jet(s)}$ final state can potentially be utilized in order to measure the summed doublet Higgsino (or analogous heavy electroweak state) decay branching fractions when such states are discovered. Observation of the Z/h branching fraction ratio, and quantification of its compatibility with unity, would probe the extent to which the Goldstone equivalence theorem can offer interesting constraints on models of new physics. The searches of interest are inherently difficult, since direct production of the Higgsino-like second lightest neutralino in the NMSSM and of the heavier neutral fermion in the singlet-doublet extension are not generically expected to exhibit very large cross sections. The additional jet(s) are useful for building more missing energy into the targeted event topology, since tagging of the leptons and $b\bar{b}$ require visible decays of Z, h. This may exhaust the mass difference between the LSP and NLSP, especially when the LSP is not massless, limiting the available missing energy.

In Sec. II, we present sample MSSM and NMSSM Higgsino scenarios that are of observational interest at the LHC, as well as a third example of a simplified fermion singlet-doublet dark matter model [4] that leaves the SM Higgs sector (and associated implications for the Goldstone equivalence manifest in the doublets' decay branchings) intact. Section III elaborates on experimental issues relevant to discrimination of the Z/h decay ratio. In order to ascertain the potential sensitivity of such an analysis of new heavy weak doublets at the LHC, the collider events in both signal and background channels are generated by Monte Carlo, and Sec. IV describes the simulation setup and assumptions. Sections V and VI detail the classification and selection optimization applicable to the various final states. We conclude in Sec. VII.

II. BENCHMARK SCENARIOS

The first benchmark scenario to be described is an MSSM construction. To be general, we choose a 70 GeV LSP mass, above $M_Z/2$, so that the tight invisible Z decay constraints may be evaded without requiring a pure bino state. A 70 GeV LSP also evades existing LHC constraints on Higgsino pair production searches [5,6]. We take the NLSPs to be Higgsinos that are relatively light, but that can still decay into the LSP and the Z, h bosons. Due to its Higgsino mixing, the LSP mass has to satisfy constraints arising from direct detection experiments, e.g., LUX [7]. We thus choose $\mu < 0$ to help suppress the LSP coupling to the Higgs, as shown in Table I.

For point I, we assume all sfermions are heavy and decouple at leading order. The wino is also assumed heavy. When $\tilde{\chi}_2^0$, $\tilde{\chi}_3^0$ are produced at the LHC, it is useful to consider a ratio of the decay branching into Z over that into h, as defined in Ref. [10],

$$\xi^{Zh} \equiv \frac{f_{\tilde{\chi}_2^0}\mathrm{BR}(\tilde{\chi}_2^0 \to \tilde{\chi}_1^0 Z) + f_{\tilde{\chi}_3^0}\mathrm{BR}(\tilde{\chi}_3^0 \to \tilde{\chi}_1^0 Z)}{f_{\tilde{\chi}_2^0}\mathrm{BR}(\tilde{\chi}_2^0 \to \tilde{\chi}_1^0 h^*) + f_{\tilde{\chi}_3^0}\mathrm{BR}(\tilde{\chi}_3^0 \to \tilde{\chi}_1^0 h^*)}, \quad (1)$$

where f is the number fraction of a specific neutralino in the signal events, and h^* denotes any (pseudo)scalar at the Higgs mass. For instance, in the NMSSM h^* can be either the Higgs scalar or the singlet pseudoscalar a_1. At all our benchmark points, the s-channel $Z^* \to \tilde{\chi}_2^0\tilde{\chi}_3^0$ process dominates pair production rates and $f_{\tilde{\chi}_2^0} \approx f_{\tilde{\chi}_3^0}$, due to a suppression in the $Z\tilde{\chi}_i^0\tilde{\chi}_j^0$ coupling for $i = j$ when $\tilde{\chi}_2^0$, $\tilde{\chi}_3^0$ are dominantly Higgsinos.

From the Goldstone theorem, $\tilde{\chi}_i^0 \to \tilde{\chi}_1^0 h \approx \tilde{\chi}_i^0 \to \tilde{\chi}_1^0 Z$ in the longitudinal Z polarization. As Z also has transverse polarization that couples to $\tilde{\chi}^0$, summing up the decay branchings of $\tilde{\chi}_2^0$, $\tilde{\chi}_3^0$ would result in comparable yet higher decay branching into Z, i.e., $\xi^{Z/h} > 1$ for $f_{\tilde{\chi}_2^0} = f_{\tilde{\chi}_3^0}$. It is worth noticing that a large $\xi^{Z/h}$ ratio can arise from a kinematic suppression when the mass gap separating the neutralinos is relatively small, as the decay into Z has a larger phase space. If point I is modified to feature a very light bino, $\xi^{Z/h}$ is modified to around 2.

TABLE I. A sample MSSM scenario with light Higgsinos. The mass spectrum and decay branchings are evaluated with Suspect2 [8] and the MSSM calculator as part of the MadGraph [9] package.

MSSM	M_1	μ	$\tan\beta$	$M_{\tilde{\chi}_1^0}$	$M_{\tilde{\chi}_2^0}$	$M_{\tilde{\chi}_3^0}$	ξ^{Zh}
Point I	71	−190	10	70	198	202	3.6

The second scenario that we discuss is a singlino LSP, Higgsino NLSP case in the NMSSM [11], whose superpotential has the following structure,

$$W_{\text{Higgs}} \supset \lambda \hat{S}\, \hat{H}_u \cdot \hat{H}_d + \frac{\kappa}{3}\hat{S}^3. \tag{2}$$

An effective $\mu = \lambda\langle\hat{S}\rangle$ term is generated when the singlet field takes a VEV, and naturalness suggest that the combination is of the order of M_Z. Note that the trilinear singlet term simultaneously generates a mass proportional to $\kappa\langle\hat{S}\rangle \equiv \kappa\mu/\lambda$. The somewhat heavy observed Higgs mass at 125 GeV receives tree level contribution from the singlet field, which argues for a larger singlet coupling λ in order to help reduce dependence on multi-TeV stops and the associated fine-tuning. Interestingly, the NMSSM allows one of the scalars (and one pseudoscalar) to be very light, if it is mainly a singlet. This extra scalar, which decays into $(b\bar{b}, \tau\bar{\tau})$ at an invariant mass outside the 125 GeV window, will be a strong indication of this model. However, if we stay in the picture that the Higgs *is* the lightest of the NMSSM scalars and contains no more than 50% singlet, the singlet cubic coupling κ would be nonvanishing. The correlations between a large λ, a small μ, a nonzero κ, and a mass gap from the LSP greater than the Higgs mass force the Higgsino dominated $\tilde{\chi}_2^0, \tilde{\chi}_3^0$ to be at least ~270 GeV. We take the first (A) and third (C) benchmarks from Ref. [10], summarized as points II and II′ in the present Table II.

We are interested in focusing on the parameter space region where the singlet (pseudo)scalars are somewhat heavier than, or comparable in mass to, the Higgs, and not kinematically distinguishable. For benchmark point II, the singlet-dominated pseudoscalar a_1 is a fair bit heavier than the Higgs, at 161 GeV. This kinematically prohibits decays of the NLSP into a_1, and the ratio $\xi^{Z/h} > 1$ thus falls within the same range as it does in the MSSM. For benchmark point II′, a_1 is slightly lighter at 119 GeV, which is very close to the h mass and can fake the Higgs boson. The total decay fraction into h and a_1 will exceed the Z fraction in this case, leading to a ratio $\xi^{Zh} < 1$ that is distinguishable from the MSSM.

The third scenario we consider is a non-SUSY BSM example with an unmodified Higgs sector, specifically the singlet-doublet fermionic (SDF) dark matter model [4]. This model extends the SM with a singlet fermion S that couples to the SM Higgs field via two heavier weak doublets D_1, D_2, which have $U(1)_Y$ charges of $-\frac{1}{2}$ and $+\frac{1}{2}$, respectively,

$$-\mathcal{L}_{\text{SDF}} = y_{D_1} S H D_1 + y_{D_2} S H^\dagger D_2 + \frac{1}{2} M_S S^2 + M_D D_1 D_2. \tag{3}$$

The new fermions S, D_1, D_2 mix via a symmetric mass matrix,

$$\mathcal{M} = \frac{a}{b}\begin{pmatrix} M_S & \frac{1}{\sqrt{2}} y_{D_1} v & \frac{1}{\sqrt{2}} y_{D_2} v \\ \frac{1}{\sqrt{2}} y_{D_1} v & 0 & M_D \\ \frac{1}{\sqrt{2}} y_{D_2} v & M_D & 0 \end{pmatrix}. \tag{4}$$

In general, the spectrum of neutral mass eigenstates $\{\chi_i^0\}$ consists of one lighter singlet-dominated state and two heavier doublet-dominated states that behave analogously to the pair of Higgsinos in supersymmetric models, though larger couplings allow for more mixing than is typically possible in the neutralino sector of the MSSM. We will focus on the parameter state where the DM χ_1^0 is light and singlet-dominated, while the two doubletlike states $\chi_{2,3}^0$ are heavier, in order to allow for the desired decays. For visual distinction, these fermions do not have a tilde (~) positioned above their symbols. The mixing angle $\tan\theta \equiv y_{D_1}/y_{D2}$ indicates the relative size of the D_1, D_2 couplings, and $y \equiv \sqrt{y_{D1}^2 + y_{D2}^2}$.

Neglecting any potential loop-order correction to the Higgs mass, the terms in Eq. (4) leave the SM Higgs sector unchanged, and the Goldstone equivalence theorem predicts similar branching fractions in the $\chi_{2,3}^0 \to \chi_1^0$, Z/h decays. Figure 1 shows the Z/h ratios associated with $\chi_{2,3}^0$ decays are approximately symmetric, up to corrections from the kinematic and mixing differences. The $ySHD$ term plays a central role in providing the NLSPs comparable decay width into Z, h (see Appendix A for details). The doublet component in the DM leads to DM-nucleon scattering via the Z boson, and the shaded regions in Fig. 1 denote the parameter space corresponding to a large DM-nucleon scattering cross section that is ruled out by LUX [7]. The gap between the two shaded areas in the right half ($\theta > 0$) of each panel identifies an allowed region of parameter space where the lightest fermion, i.e., the DM candidate, mass becomes sufficiently light that LUX loses sensitivity and cannot rule out the scenario. The discontinuity at $\theta \approx -0.03\pi$ occurs because the pair of doubletlike states become Dirac once more at that point, resulting in a phase shift in the rotation matrix across the transition. We refer to Ref. [4] for the nucleon scattering cross-section calculation, and other phenomenological studies of this model.

Table III provides an SDF benchmark (point III). The mixing angle is chosen to be $\theta = -0.05\pi$, where the LSP-nucleon scattering is suppressed and the coupling y can take relatively large values. Similar to the MSSM, point III also gives rise to a higher decay branching into Z, as predicted by the Goldstone equivalence theorem. This

TABLE II. A pair light Higgsino NMSSM benchmark points, exhibiting over (II) and under (II′) production of the Z relative to the h.

NMSSM	λ	κ	μ	$\tan\beta$	m_{a_1}	$m_{\tilde{\chi}_1^0}$	$m_{\tilde{\chi}_2^0}$	$m_{\tilde{\chi}_3^0}$	ξ^{Zh}
Point II	0.8	0.25	220	2.9	161	143	270	270	2.1
Point II′	0.8	0.25	230	2.9	119	150	279	279	0.7

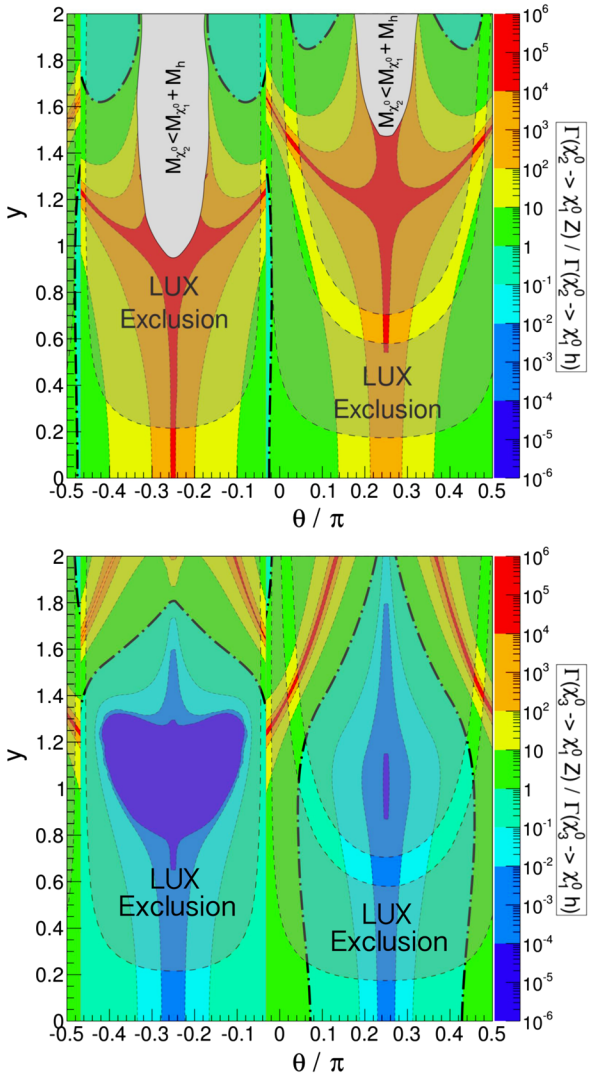

FIG. 1. Near symmetric branching ratio of $\chi^0_{2,3}$ decays in the SDF dark matter model. $M_S = 50$ GeV and $M_D = 200$ GeV throughout.

shows that, in the simplified picture of weak doublet fermion decays, the unaltered Higgs sector also yields a ratio $\xi^{Z/h} > 1$; this stands in contrast to the situation where a new field masking the Higgs is additionally present, as in the case of NMSSM. However, similar final states and a similar ξ ratio make this model difficult to distinguish from other constructions like the MSSM, underscoring a need for caution in the interpretation of results that may be mutually associable with a degeneracy of underlying structures. In this case, more knowledge about the model's particle spectrum will be needed.

TABLE III. Benchmark SDF dark matter point.

SDF	y	θ	M_S	M_D	$M_{\chi^0_1}$	$M_{\chi^0_2}$	$M_{\chi^0_3}$	ξ^{Zh}
Point III	0.4	-0.05π	72	189	70	201	203	3.0

III. EXPERIMENTAL CONSIDERATIONS

Pair production of the various heavy weak doublet candidates identified with the aforementioned scenarios constitutes a potentially viable search channel at the LHC. The decay of these doublets and the subsequent decay of the associated Z/h boson products lead to final states that contain leptons and b-tagged jets, plus some amount of missing transverse energy $\not{E}_{\mathrm{T}}$, and (optionally) additional jets.

The Z boson will decay dominantly to hadrons (70%), including a 15% share to just the $b\bar{b}$ final state. Invisible decays account for 20% of the branching, and the final 10% is shared among the three lepton pair production modes $\ell\ell$. There is no intrinsic preference for or against τ production in this mode, but we will focus on the selection only of light lepton (e, μ) flavors because they have a much higher detection efficiency, and a lower fake rate. The Higgs boson h will be reconstructed from its decay into $b\bar{b}$, at a large branching which is under correction from the size of $\tan\beta$ in supersymmetric models. If a $\sim$125 GeV NMSSM singlet pseudoscalar emerges, it dominantly decays into $b\bar{b}$ with a branching near 100%.

Light leptons will not be produced directly at any appreciable rate by the decays of the Higgs, although there may be leptonic decays arising from its direct decay products, with light opposite-sign mixed-flavor pairs (along with the associated missing neutrinos) represented in the final state at a typical branching of about 1% each (for a SM Higgs) via the WW^* and $\tau\tau$ channels. These rates may be further discriminated from the direct decays of the Z by demanding same flavor combinations with kinematic reconstruction of the parent mass.

From the decay of mixed Z/h pairs, the targeted final states will therefore correspond to four leptons $\ell\ell\ell\ell$, four b tags $b\bar{b}b\bar{b}$, or a mixed state $\ell\ell b\bar{b}$. The lepton production channels will be associated with Z boson decays, and the b-tag production channels will be dominantly associable with decays of the Higgs (and Higgs-like states). Two out of the three described signals must be measured in order to ascertain the parent doublets' total decay branching ratio into Z and h.

The four-lepton channel has a substantial SM background of vector bosons plus jets, where the vector boson, e.g., the Z, decays leptonically and jet mismeasurement provides a source of missing energy. Contributions include t-channel vector pair production, and s-channel single production of a vector resonance with one leg of the ensuing leptonic decay further radiating a second off-shell vector; our simulation reflects a strong contribution from the former. These backgrounds can be efficiently controlled by a $\not{E}_{\mathrm{T}}$ cut and by invoking variables designed to discriminate against the spurious appearance of $\not{E}_{\mathrm{T}}$ that is faked by jet mismeasurement. Profitable selection alternatives will be discussed in Sec. V.

By comparison, the two- and four-b-jet channels are mainly affected by a more severe SM $t\bar{t}$ background, where the two natural b quarks from top decay may be readily accompanied by additional jet-faked b's. Given the crowded final state, the rate of fake b jets is non-negligible, and this background remains quite severe even after a $b\bar{b}$ invariant mass window cut is imposed. Compared to the 4ℓ final state, channels involving fewer leptons (and correspondingly higher b-tag requirements) will thereby turn out to have substantial disadvantages with regards to detection efficiency, as will be shown in the analysis of specific event selection alternatives in Sec. VI. If the LSP is massless, Run I of the LHC sets limits in the $4b$ channel, but there are no existing limits for a massive LSP scenario.

When the mass gap between the decaying doublets and the LSP is close to (or less than) 125 GeV, the decay into h may become kinematically suppressed, leading to Z-dominated final states with the observable consequence that $\xi^{Zh} > 1$. Additionally, even when decay into h is allowed, it can still be very difficult in this regime to boost an appreciable quantity of $\not{E}_{\mathrm{T}}$. It is helpful then to tag on initial state radiation (ISR) jets in order to boost the overall $\not{E}_{\mathrm{T}}$ of the visible system, but two ISR jets are observed in simulation (for the point II benchmark specifically) to cost a .5 magnitude order in production cross section.

Further details regarding the mode of simulation, the specific mechanisms available for controlling various backgrounds, and the expected visibility of the three targeted final state signal topologies at the $\sqrt{s} = 14$ TeV LHC are provided in the following sections. We will not attempt a detailed extraction of the ξ^{Zh} ratio from simulated collider data in this work, but will instead direct attention toward the preliminary task of establishing the signal. We will reference NMSSM benchmark II for concreteness, and comment on the extrapolation of results to other benchmark scenarios.

IV. EVENT GENERATION AND SELECTION

Signal and the standard model (SM) background Monte Carlo event samples, including parton showering and fast detector simulation, are generated via the standard MadGraph5/MadEvent [9], Pythia [12], Delphes 3 [13] chain. MadEvent is configured, in conjunction with Pythia, to use MLM matching. The Delphes 3 detector simulation employs a standard LHC-appropriate parameter card, with jet clustering performed using the anti-kt algorithm. Selection cuts and computation of collider observables are implemented within AEACuS 3.15 [14,15] using the instructions in card VI, as exhibited in Appendix B. At the preselection stage, jets (including b-tagged jets) are accepted with a transverse momentum $P_{\mathrm{T}} > 30$ GeV, up to a pseudorapidity magnitude of $|\eta| < 2.5$ (although wide jets $|\eta| < 5.0$ are employed for limited purposes such as counting of single-track jets). Leptons, including hadronic taus, are accepted with $P_{\mathrm{T}} > 10$ GeV and $|\eta| < 2.5$. Light leptons (e, μ) are required to maintain a mutual isolation of $\Delta R > 0.3$.

Background candidates simulated here are the inclusive production of $t\bar{t}$ with zero to two jets, the inclusive production of two vector bosons (meaning W and/or Z) with zero, one, or two jets, as well as single W- or Z-boson production including zero to four initial state jets. The single vector channels exhibit very large production cross sections, around 2 orders larger than the corresponding $t\bar{t}$ background, and the approximately 15 million events considered for each case remain a substantial undersampling. Approximately three million events were sampled for the $VV +$ jets background, corresponding to around 20 fb^{-1} of integrated luminosity. More than 60 million events were sampled for the $t\bar{t} +$ jets background, corresponding to around 100 fb^{-1} of integrated luminosity. For signals, we have simulated around 25 million events for the NMSSM benchmark II point, likewise inclusively considering zero to two jets, which corresponds to an integrated luminosity approaching half a million events per femtobarn.

Signal events are preclassified into three nonoverlapping categories based on the count of light leptons (e, μ), along with a complementary threshold for the count of heavy-flavor (b-tagged) jets, as stipulated at the bottom of the card VI instructions. Category I contains at least four leptons, but has no b-tagging requirement. Category II contains either two or three leptons, and at least two b jets. Category III contains either zero or one lepton, and at least four b jets. There is significant attenuation of both signal and background by these preliminary topological cuts, as demonstrated in Table IV. Category I is intrinsically low background, and the signal already competes well here, being of the same magnitude order as the isolated $t\bar{t} +$ jets and $VV +$ jets components. Categories II and III are dominated by the $t\bar{t} +$ jets background, which shall prove quite difficult to reduce while retaining any appreciable portion of the already meager signal. Additionally, we preemptively summarize in Table V the supplementary event selection optimizations and cut flow for each of these event categories, which will be established in the following sections.

TABLE IV. Matched production and residual effective cross section (fb) at the LHC14 are tabulated for the three targeted final state event topologies, reported individually for the $t\bar{t} +$ jets and $VV +$ jets backgrounds, as well as the benchmark point II NMSSM signal.

Selection	$t\bar{t} +$ jets	$VV +$ jets	$W/Z +$ jets	Signal
Matched production	613,000	150,000	2.27×10^8	53
Cat I ($4^+ e/\mu$, 0^+B's)	0	11.6	0	0.037
Cat II ($2-3e/\mu$, 2^+B's)	3590	12.8	62.6	0.130
Cat III ($0-1e/\mu$, 4^+B's)	1430	6.43	147	0.114

TABLE V. Summary of optimized secondary event selections employed for each of the three targeted final state event topologies. Also presented are the (sequential flow) percentages cut of residual events for the background (B) and signal (S), respectively, where B invokes the unified SM components $t\bar{t}+$ jets, $VV+$ jets, and $W/Z+$ jets. Statistics for the baseline topology of each event selection category were presented in Table IV.

Cat I ($4^{+}e/\mu$, 0^{+}B's)	% (B,S)	Cat II ($2-3e/\mu$, 2^{+}B's)	% (B,S)	Cat III ($0-1e/\mu$, 4^{+}B's)	% (B,S)
τ veto	(0.4,0.7)	τ Veto	(1.1,1.2)	2 leading B jets	(50,28)
b-jet veto	(0.4,1.5)	1^{+} hadronic Z/H	(61,21)	e/μ veto	(12,0.8)
$\not{E}_{\mathrm{T}}/\sqrt{H_{\mathrm{T}}} > 6.0$ GeV$^{1/2}$	(100,64)	1^{+} leptonic Z	(95,27)	τ veto	(5.7,2.4)
		1-track jet veto	(1.3,1.6)	2^{+} hadronic Z/H	(58,34)
		$\Delta R < 2.0$	(56,40)	6^{+} jets veto	(52,13)
		$\not{E}_{\mathrm{T}}/\sqrt{H_{\mathrm{T}}} > 3.0$ GeV$^{1/2}$	(57,28)	1-track jet veto	(2.4,1.4)
				$\not{E}_{\mathrm{T}}/\sqrt{H_{\mathrm{T}}} > 3.0$ GeV$^{1/2}$	(72,35)

It should be emphasized before proceeding that the baseline NMSSM matched production cross section (~50 fb) provided in Table IV is for the particular neutralino mass $M_{n_{2,3}} \sim 270$ GeV associated with benchmark II, which has been selected as the default scenario for our collider study. The cross section can be a quite a bit larger when the associated doublets are lighter, as can occur in the MSSM and in the SDF models. If the relevant mass scale, e.g., for the Higgsino-type MSSM neutralino or for the SDF doublet, is reduced from 270 to around 200 GeV, an increase in the Higgsino pair-production cross section by a factor of order 5 can generically be expected [16,17]. In Fig. 2, we preemptively summarize the optimized visibility of each signal region at a luminosity of $3,000$ fb^{-1} as a rescaled function (statistical errors only) of the postcut cross section. Kinematic cut efficiencies are expected to be less affected by scaling when the mass gaps between the LSP and NLSP(s) remain as represented by the benchmarks. The scaling is affected by both the Higgsino production rate and the ratio $\xi^{Z/h}$ that determines the neutralinos' branching into each final state category. Benchmark II, with $\xi^{Z/h} = 2.1$, thus inherits a greater share of leptonic final states. For a model with a low $\xi^{Z/h}$, like benchmark II, a higher branching ratio into $b\bar{b}$ would then enhance the $bbll$ significance (relative to $4l$). The four-lepton (category I) signal region is found to be highly visible, whereas the mixed lepton plus b-jet signal region (category II) is conditionally visible, and the four-b-jet signal region (category III) projects low visibility. The applicable event selection strategies in each event category are developed in detail in the subsequent sections.

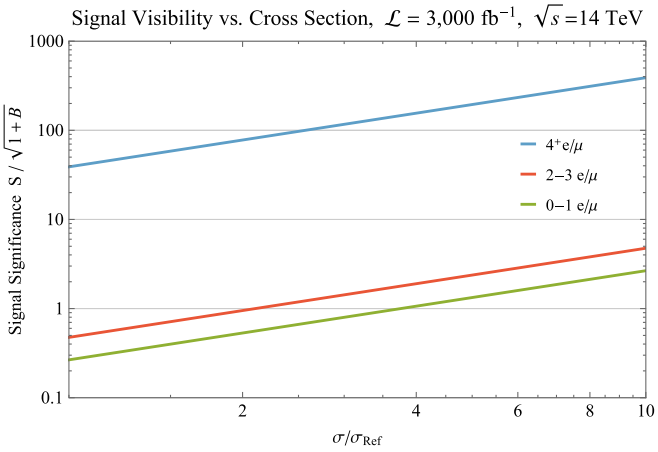

FIG. 2. The signal significance metric $S/\sqrt{1+B}$ is projected for each of the targeted final state topologies at a luminosity of $3,000$ fb^{-1} at the $\sqrt{s} = 14$ TeV LHC, using statistical errors on the simulated background estimation only. Collider modeling is based on NMSSM benchmark II, which features 270 GeV Higgsinos and a Z/h ratio of $\xi^{Z/h} = 2.1$. The horizontal axis represents numerical scaling of the production cross section relative to this benchmark. The optimized event selections employed are summarized in Table V. Supplementary cuts on $\not{E}_{\mathrm{T}}$ are not considered here, although this could become a favorable strategy at very large luminosity or cross section for the middle $2\ell 2b$ scenario, as elaborated in Sec. VI. Notice that the scaling of the postcut σ depends on both the Higgsino production cross section and the neutralino decay branching into the specific final state categories. Particularly at large luminosity, systematic errors in the background will likewise be important, summed in quadrature with the statistical fluctuation of the background.

V. REFINING THE FOUR-LEPTON SIGNAL

A natural final state to target for models similar to the NMSSM benchmark under consideration is the category I four-lepton topology. This final state has been carefully studied at the LHC [18]. The question of whether it is possible to improve the discrimination of signal from background is investigated in the present section. To begin, a sequence of plots is shown that compare the normalized event shape distributions of the signal and background for several observables. All plots have been generated with the RHADAMANTHUS 1.2 [15] software package. The single vector backgrounds have been integrated with the di-boson production channel. Moderate bin smoothing is employed.

Events featuring $t\bar{t}+$ jets production are generally unable to legitimately yield more than two leptons, and

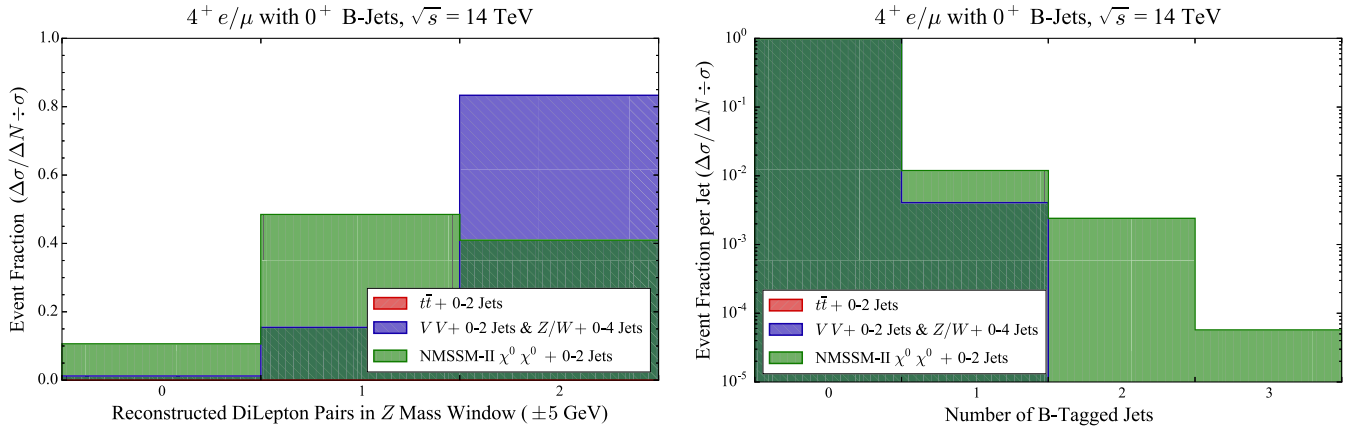

FIG. 3. Signal and background event shapes are compared for the final state topology with 4^+ light leptons (category I). The $t\bar{t}$ background component delivers no appreciable contribution to this final state. Left: Over 90% of the signal features a reconstructed OS-LF dilepton in the Z-boson mass window (92 ± 5) GeV. About half of the signal reconstructs precisely a single Z, whereas almost 85% of the unified vector backgrounds are actually observed to reconstruct two pair. Right: Neither the signal nor the dominant VV + jets background are likely to be tagged for a b jet at beyond the percent level, although likelihood for the signal is somewhat greater by comparison.

simulation suggests that the likelihood of this background faking the targeted four-lepton final state may likewise be discounted. The leading vectors plus jets background is capable of producing this event topology directly, although the branching fraction for Z to 4ℓ is at the 10^{-6} order [18]; the four-lepton requirement essentially rules out final states with neutrinos, and any missing transverse energy associated with this production mode will typically arise from measurement error. This observation suggests that collider variables designed to root out fake missing energy signals may be very helpful here, such as the $\not{E}_{\mathrm{T}}$-jet angular difference $\Delta\phi$ [19] (applied as the minimal azimuthal separation between the missing transverse energy and the leading and b-tagged jets) and the missing energy significance $\not{E}_{\mathrm{T}}/\sqrt{H_{\mathrm{T}}}$.

In Fig. 3, the signal is differentiated from the leading VV + jets background as more likely to feature precisely one candidate Z boson, defined as an OS-LF dilepton pair with an invariant mass of 92 ± 5 GeV (left panel). More specifically, the unified vector backgrounds are more likely, by about 6 times, to contain two pairs rather than one, whereas the signal is observed to contain 0, 1, 2 reconstructible Z bosons in approximately 10%, 50%, 40% of events, respectively. Neither the signal nor leading background are likely beyond the percent level to feature b jets, although the signal events are slightly more likely (right panel). Similarly, the signal generally contains no hadronic taus. It is also noted that the signal production cross section for two jets is smaller by a factor of almost 4 than the matched inclusive cross section with zero to two jets; the signal is likewise not very jetty in character.

In Fig. 4, the signal and vectors plus jets background are observed to behave consistent with the respective expectations for a legitimate and measurement-induced missing energy source. Specifically, the background favors small $\Delta\phi$, with $\not{E}_{\mathrm{T}}$ well aligned to a hard jet, whereas the signal is characterized by larger $\Delta\phi$ angles, indicating less correlation between the $\not{E}_{\mathrm{T}}$ and hard jet directionality (left panel); this variable is best suited for application to signals such as the one under consideration that are not overly jetty. Likewise, the quantity of missing transverse energy observed in signal is generally a much more substantial multiplier of the estimated uncertainty $\sqrt{H_{\mathrm{T}}}$ in the hard event scale (right panel).

Based upon these observations, supplementary event selection may be performed, corresponding to a requirement of $\not{E}_{\mathrm{T}}/\sqrt{H_{\mathrm{T}}} > 6.0\ \mathrm{GeV}^{1/2}$; this cut essentially eliminates the vectors plus jets background in our simulation, while retaining approximately 40% of the signal. Additional discrimination may be achieved by requiring no more than one OS-LF di-lepton invariant mass reconstruction within 5 GeV of the Z boson, or by requiring $\Delta\phi > 2$, although the original selection is sufficient in our simulation to squelch background, while retaining the largest fraction of an already tenuous signal strength. It will typically do no harm to additionally impose a veto on b jets and hadronic taus; although this does not strengthen discrimination against the vector backgrounds, it may further harden the exclusion against fakes from channels such as $t\bar{t}$ + jets. In fact, it will suppress the signal by no more than about ten percent to rule out events with more than one jet of any type.

In Fig. 5, the absolute event counts attributable to the signal and background components are compared as a function of the missing transverse energy $\not{E}_{\mathrm{T}}$ cut threshold for an integrated luminosity of 300 fb^{-1}; the left-hand panel corresponds to the raw category I preselection,

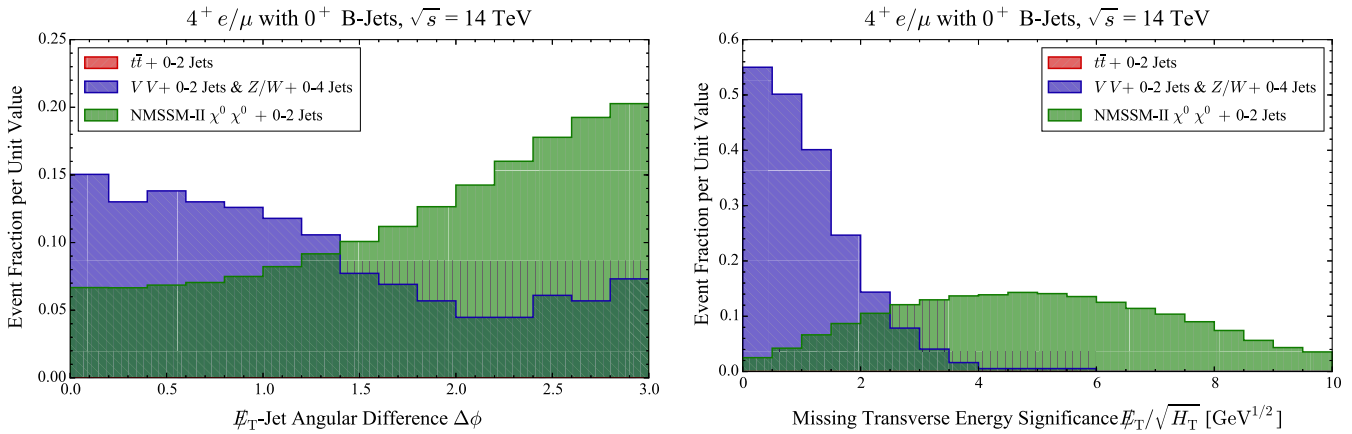

FIG. 4. Signal and background event shapes are compared for the final state topology with 4^+ light leptons (category I). The $t\bar{t}$ background component delivers no appreciable contribution to this final state. Left: The leading vectors plus jets background relies on jet mismeasurement in order to generate missing energy, and the $\not{E}_T$ azimuthal direction is thereby here observed to be much more strongly correlated (smaller $\Delta\phi$) with the direction of a single hard jet than is the case for the signal's legitimate missing energy. Right: Likewise, the quantity of missing transverse energy observed in signal is generally a much more substantial multiplier of the estimated uncertainty $\sqrt{H_T}$ in the hard event scale.

whereas the described secondary event selections are enacted in the right-hand panel. In this case, the residual discrimination power of the missing transverse energy variable is apparent, with the background rate observed to drop below the signal rate in the vicinity of 175 to 200 GeV. However, the absolute signal rate remains rather low at the studied luminosity in this scenario, at close to the unit level. The effect of enforcing a hard cut on the significance estimator $\not{E}_T/\sqrt{H_T} > 6.0$ GeV$^{1/2}$ is apparent in the right-hand panel, where backgrounds are eliminated while retaining about four signal events at the simulated luminosity and cross section. Even after a mild cut on the missing transverse energy, no greater than about 100 GeV, the projected signal significance is in a favorable range close to 4.

VI. REFINING THE 2–3 LEPTON PLUS 2^+ *B*-JET AND 4^+ *B*-JET SIGNALS

The category II event classification with two to three leptons and two or more b jets has the disadvantage of a final state topology that is readily mimicked by the dual leptonic decay of W bosons from $t\bar{t}$ production. With a moderate fake rate for b jets, the background is likewise heavily represented in the category III (0–1 lepton with 4 or more b-jet) event topology.

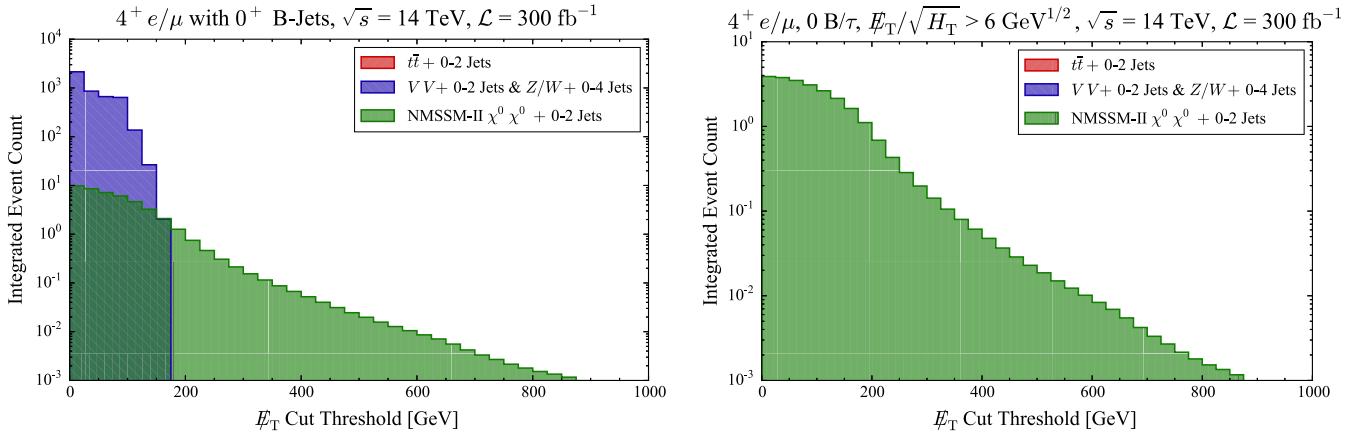

FIG. 5. Signal and background integrated event counts are compared for the final state topology with 4^+ light leptons (category I) at a luminosity of 300 events per femtobarn as a function of the missing transverse energy $\not{E}_T$ cut threshold. Left: The raw event categorization is intrinsically low background, although a weak signal may still struggle to compete at low missing transverse energy. Right: Enacting the secondary event selections ($\not{E}_T/\sqrt{H_T} > 6.0$ GeV$^{1/2}$, 0 τ, 0 B's) suggested by Figs. 3 and 4 preferentially suppresses the background, to a point approaching elimination. There is then no residual necessity for large missing energy, although neither is a modest cut in the vicinity of $\not{E}_T > 100$ GeV strongly disfavored.

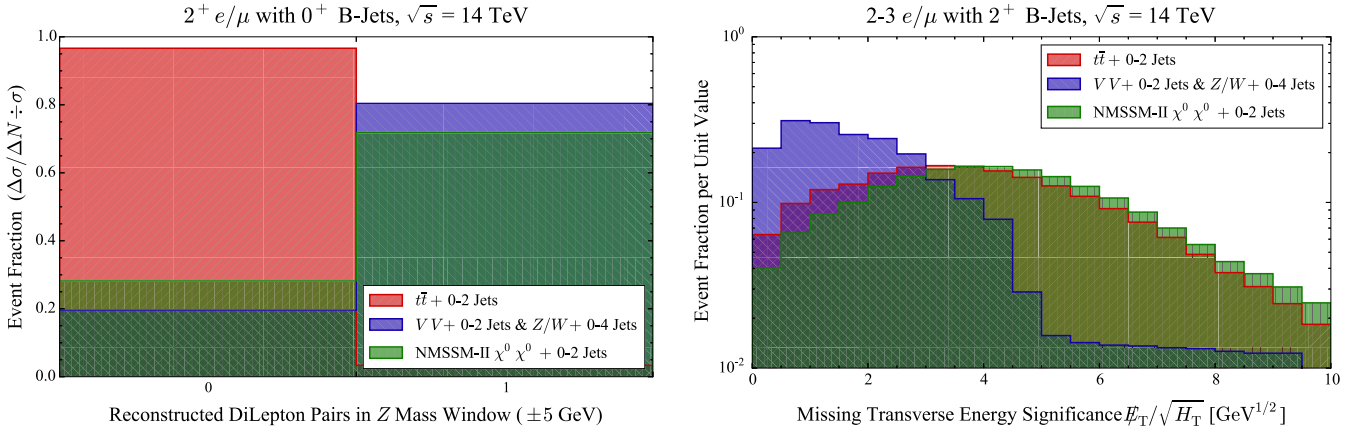

FIG. 6. Signal and background event shapes are compared for the final state topology with 2–3 light leptons and 2^+ b jets (category II). Left: Around 70% of the signal features an OS-LF dilepton pair with an invariant mass of 92 ± 5 GeV, whereas the same holds true for only approximately 3% of the $t\bar{t}$ background component. Right: The relative (dimensionful) significance of the missing transverse energy as a numerical ratio of $\not{E}_T$ to the square-root of the event scale M_T (both in GeV) is substantially larger for the signal (as well as for $t\bar{t}$) than the vector background components.

Moreover, the light SUSY electroweak sector considered for the signal benchmarks does not typically yield a quantity of missing energy that is sufficiently large to substantially distinguish it from the background. See Figs. 8 and 11, left-hand panels, for a comparison of the raw event residuals as a function of missing transverse energy cut threshold at a luminosity of 300 fb^{-1}. The signal is observed to be dwarfed in both cases by around 4 magnitude orders. A large variety of kinematic discriminants and specialized discovery variables have been tested in an effort to identify handles effective for the isolation of signal events.

Considering first category II, it is apparent in the left-hand panel of Fig. 6 that the signal is emphasized by insisting that an available pair of light OS-LF leptons kinematically reconstruct the mass of a Z boson (left panel). The right-hand panel of Fig. 6 demonstrates that the $\not{E}_T$ significance variable is again effective at curtailing the vectors plus jets background, although it is of limited efficacy against the $t\bar{t}$ + jets background; we shall select the relatively more modest implementation $\not{E}_T/\sqrt{H_T} > 3.0$ GeV$^{1/2}$ in order to not sacrifice too much signal. Figure 7 shows a similar preference for hadronic (b-jet) reconstruction of a particle in the Z/Higgs mass window (left panel), with a narrow constituent separation in ΔR (right panel); a cut $\Delta R < 2.0$ will be selected. As marginal cuts we will opt to also veto single-track jets and hadronic τ's. Figures 8 compare the signal and

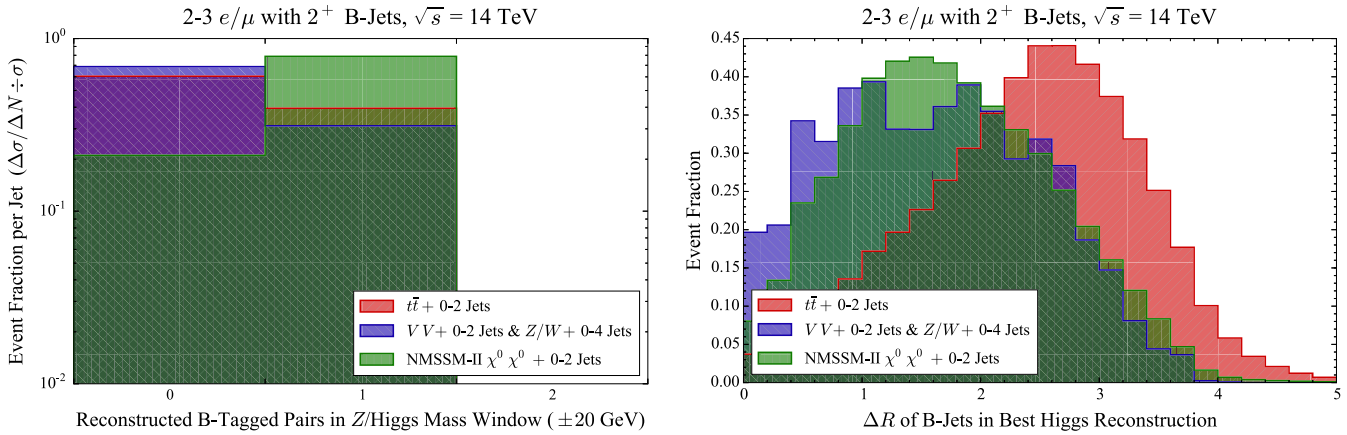

FIG. 7. Signal and background event shapes are compared for the final state topology with 2–3 light leptons and 2^+ b jets (category II). Left: About 80% of the signal features a reconstructed b-Jet pair in the Z/H-boson mass window (92–20 GeV to $126 + 20$ GeV), whereas the same holds true for just 30%–40% of the unified background components. Right: The angular separation ΔR of the pair of jets that come closest by invariant mass to reconstructing a Higgs is systematically smaller for the signal than the $t\bar{t}$ background component.

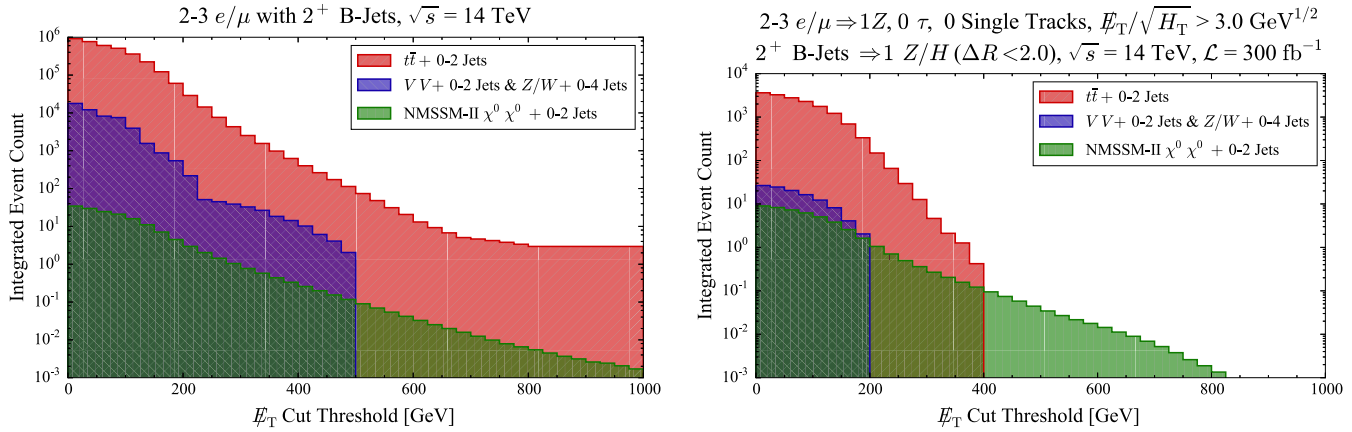

FIG. 8. Signal and background integrated event counts are compared for the final state topology with 2–3 light leptons and 2^+ b jets (category II) at a luminosity of 300 events per femtobarn as a function of the missing transverse energy $\not{E}_T$ cut threshold. Left: The raw event categorization reveals daunting background domination by $t\bar{t}$ + jets, with no substantive improvement in the signal-to-background ratio at large values of the missing energy. Right: Enacting the secondary event selections (0 τ, 1 leptonic Z, 0 single-track jets, 1 hadronic Z/H with $\Delta R < 2.0$, and $\not{E}_T/\sqrt{H_T} > 4.0$), the signal-to-background ratio is improved by 2 or 3 magnitude orders (more at larger $\not{E}_T$ cuts), although it remains apparently intractable at the studied luminosity and signal cross section.

background event residuals before (left) and after (right) these secondary selections. The background is reduced by more than 2 magnitude orders, while the signal is reduced only by a simple factor of 3 or 4. However, the ratio still heavily favors the $t\bar{t}$ + jets background component, by 2 to 3 orders of magnitude (less at higher $\not{E}_T$ cut thresholds). The positive response to a cut on missing energy suggests that this could be an effective strategy if very large luminosities and/or enhanced signal cross sections were available.

Potential discriminants tested but found to be of limited help in this case include M_{T2} (the "s-transverse mass") [20,21], M_{T2}^W [22], the jet and dilepton-Z transverse energy balance ΔE_T [23], the razor variables [24,25], the α_T ratio [26,27], the "biased" azimuthal difference $\Delta\phi^*$ [28], the lepton W-projection L_P [29,30], and various transverse thrust and event shape statistics [31–34].

Category III presents similarly in many regards, and faces the same central obstacle that the hadronic event shape is excessively similar to the background. A similar preference is observed for a mild cut on the missing energy significance $\not{E}_T/\sqrt{H_T} > 3.0$ GeV$^{1/2}$, and we again opt to veto on hadronic τ's and single-track jets. Distinctions are observed in Fig. 10, which argues for trimming the total number of jets to no more than five with the leading pair necessarily b-tagged, and in Fig. 9, which

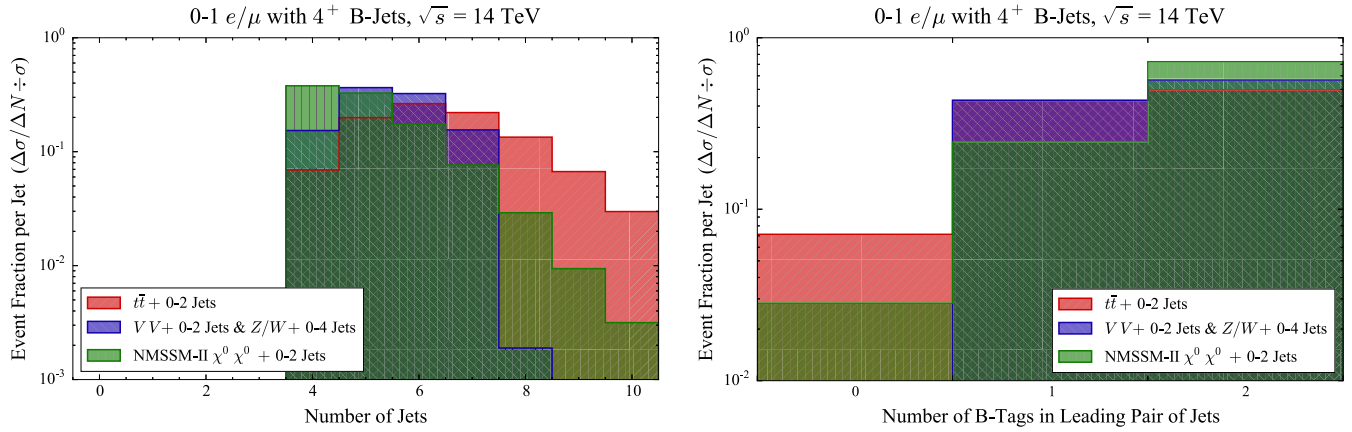

FIG. 9. Signal and background event shapes are compared for the final state topology with 0–1 light leptons and 4^+ b-jets (category III). Left: The $t\bar{t}$ background is generally jettier than the signal, with a larger fraction of events at six or more jets. Right: The leading pair of signal jets is somewhat more likely to be b-tagged than the leading pair of jets in the $t\bar{t}$ background, one or more of which are likely to be initial state radiation.

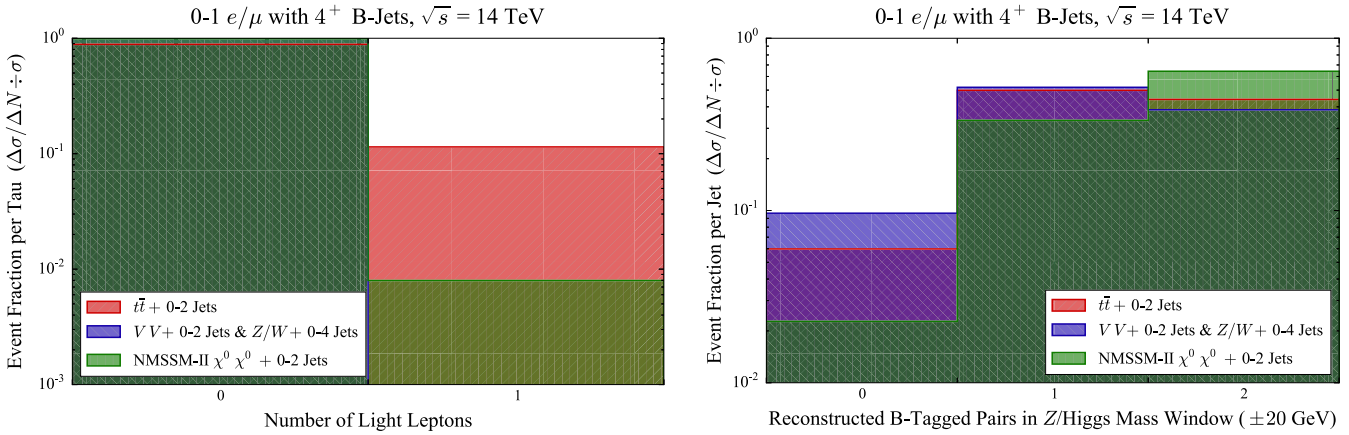

FIG. 10. Signal and background event shapes are compared for the final state topology with 0–1 light leptons and 4^+ b jets (category III). Left: The $t\bar{t}$ background is substantially more likely to retain a single lepton than the signal. Right: Around 65% of the signal features two reconstructed b-jet pairs in the Z/H-boson mass window (92–20 GeV to 126 + 20 GeV), whereas the same holds true for just around 40%–45% of the $t\bar{t}$ (vector) background components.

argues for vetoing light leptons and insisting on two hadronic (b-tagged jet) kinematic reconstructions in the Z/Higgs window. Combinatoric backgrounds reduce the efficacy of a cut on angular separation for the best mass reconstruction in this case. Figures 11 compares the signal and background event residuals before (left) and after (right) these secondary selections. The background is reduced here by around 1.5 magnitude orders, while the signal is reduced by a factor close to 3. However, the ratio still heavily favors the background, by about 3 orders of magnitude, irrespective of a cut on missing transverse energy.

Figures 12 evaluate signal-to-background event significance, using the metric $S/\sqrt{1+B}$, as a function of the missing transverse energy cut threshold for the category II (left) and III (right) final state topologies, applying the described optimizations at luminosities of 300 and $3,000$ fb^{-1}, for the baseline cross section of the benchmark II model and also for a hypothetical spectrum that is sufficiently more light to engender a 1 magnitude order increase in the production cross section. When both scale factors are invoked, it appears possible to resolve a significant signal for the category II final state topology, providing a crucial second data point (in conjunction with the highly visible first category) for reconstruction of the model. Even granting both factors, the category III final state topology remains difficult to substantially disentangle from the background.

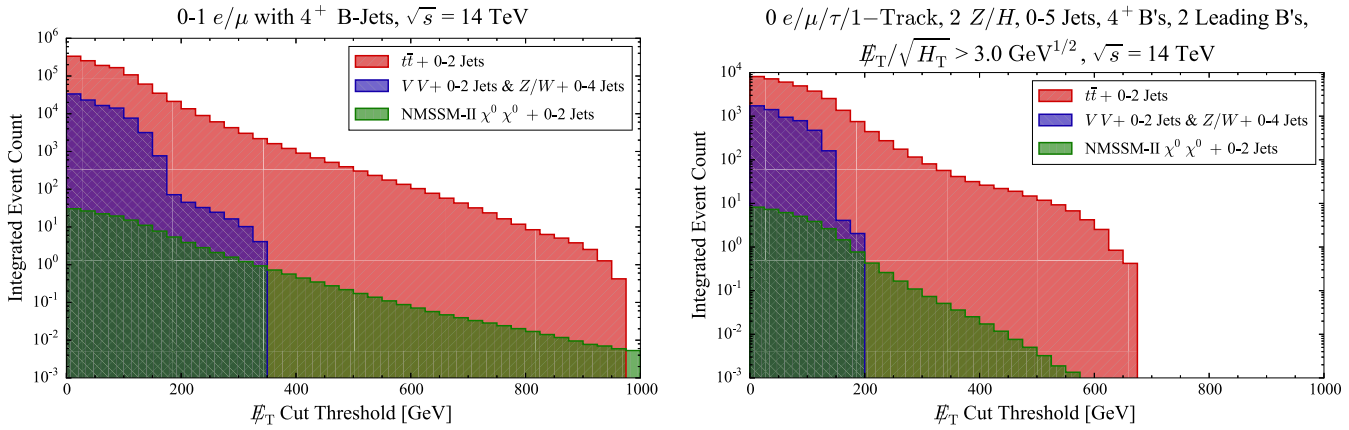

FIG. 11. Signal and background integrated event counts are compared for the final state topology with 0–1 light leptons and 4^+ b jets (category II) at a luminosity of 300 events per femtobarn as a function of the missing transverse energy $\not{E}_T$ cut threshold. Left: The raw event categorization reveals daunting background domination by $t\bar{t}$ + jets, with no substantive improvement in the signal-to-background ratio at large values of the missing energy. Right: Enacting the secondary event selections (0 e/μ, 0τ, 0–5 total jets, 2 leading b jets, 0 single-track jets, 2 hadronic Z/H, and $\not{E}_T/\sqrt{H_T} > 4.0$), the signal-to-background ratio is improved by around a magnitude order, although it remains apparently intractable at the studied luminosity and signal cross section.

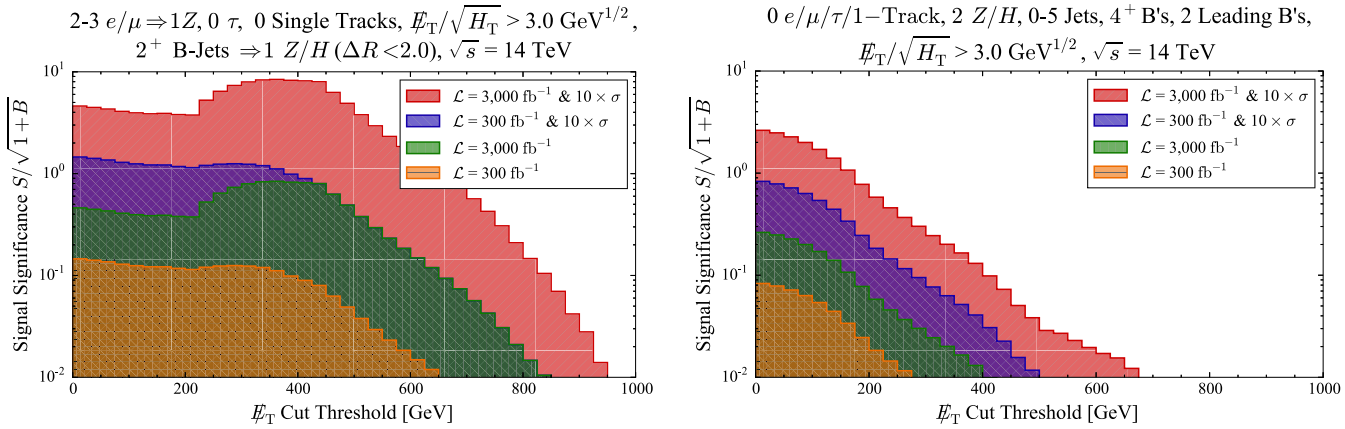

FIG. 12. The signal to background significance metric $S/\sqrt{1+B}$ is evaluated as a function of the missing transverse energy cut threshold for the category II (Left) and III (Right) final state topologies, applying the optimizations described in the right-hand panels of Figs. 8 and 11. Four contours are shown, corresponding to luminosities of 300 and 3,000 fb^{-1}, for the baseline cross section of the benchmark model and also for a hypothetical spectrum that is sufficiently more light to engender a 1 magnitude order increase in the production cross section. Only by conspiracy of both factors may a significant excess be observed, and then only for category II. In this former case, a harder cut on $\not{E}_T > 400$ GeV is suggested if luminosity and cross section are large enough to support it, in which case background is deeply contained and the signal is quite visible. By contrast, in the latter case similarities in the signal and background missing transverse energy shapes render a substantive $\not{E}_T$ cut ineffective.

VII. DISCUSSION AND CONCLUSIONS

In this paper, we investigated decays from heavy Higgsino-like weak doublets into Z, h bosons and (small) missing energy. As examples, we considered the MSSM, NMSSM and a singlet-doublet extension of the SM featuring a DM candidate that is capable of explaining the observed relic density after satisfying direct detection constraints. The NMSSM is well motivated by its natural accommodation of the 125 GeV Higgs and a weak scale value of μ.

Signals from the MSSM, NMSSM and the singlet-doublet extension will be similar; i.e., we will expect to find decays into Z, h plus missing energy that cascade into final states with 4ℓ, $2\ell 2b$ and $4b$ plus missing energy. Leptonic products will be dominantly associated with decays of the Z, whereas decays of the Higgs will be associated dominantly with heavy flavor jets. Establishing two of the prior three final states would potentially provide a mechanism for quantifying the Z to h ratio, which may in turn assist in discriminating between specific models exhibiting the described spectral features. In particular, observation of this ratio will clarify the manner in which the Goldstone equivalence theorem is manifest within and places constraint upon new physics. The ratio of Z to h production in Higgsino-like decays would be somewhat greater than 1 in the case of the MSSM and the singlet-doublet extension, since the net Z rate includes also the contribution of transverse polarizations. By contrast, in the NMSSM, the lighter neutralinos can decay into another state a, which can naturally be close to the light Higgs mass, which masquerades as the Higgs in decays and gives rise to a Z/h ratio that is smaller than 1 by its.

We explored the visibility of the 4ℓ, $2\ell 2b$ and $4b$ final states, which are useful to establishing the Z/h ratio, at the 14 TeV LHC. If heavy colored particles are to be probed at the LHC, then the lighter MSSM and NMSSM neutralinos and charginos (or their new fermion counterparts) will likewise be within reach for direct production. However, the reach for these neutralinos and new fermions is not very high, and existing bounds vanish rapidly for scenarios with a massive lightest neutralino/fermion. We selected a representative NMSSM benchmark within this class of models for detailed collider simulation, with Higgsino next-to-lightest neutralinos around 270 GeV, a singlino lightest supersymmetric particle around 140 GeV, and a light pseudoscalar around 160 GeV. Leading backgrounds were also simulated, and various event selection scenarios were tested in an effort to optimize the targeted signals. The inclusion of one to two initial state jets can be helpful in providing some additional boost to the visible system, although low signal rates, lightness of the invisible final state, and narrowness of the mass hierarchy were found to limit the efficacy of hard cuts on missing energy. The four-lepton signal region is substantially visible, with just 300 fb^{-1} of integrated luminosity proving almost sufficient for a 5σ level discovery of the benchmark model. For the same masses, the $2\ell 2b$ and $4b$ final states contend with standard model backgrounds that prove difficult to reduce. Discovery is possible in the $2\ell 2b$ topology if the benchmark cross section is elevated by a factor of around 10, in conjunction with an elevation of the luminosity to the order of 3000 fb^{-1}. Visibility of the $4b$ topology would seem to require a new collider environment, with substantially upgraded luminosity and/or center-of-mass energy.

It appears that it will be possible for the LHC to establish (in the 4ℓ channel) the studied class of models, where only lighter weak fermions exist around the electroweak scale, where the mass gap separating the dark matter candidate from the next-to-lightest states is not much larger than ∼125. For the lightest of these scenarios, and utilizing high luminosities, it seems further possible that the LHC will be able to also confront the $2\ell 2b$ channel, allowing for direct discrimination of the Z to h ratio in decays of a Higgsino-like state. These observations would function as a probe of the manner in which the new physics manifests the Goldstone equivalence theorem and would provide the opportunity to distinguish between the NMSSM and models such as the MSSM or the singlet-doublet extension of the SM.

ACKNOWLEDGMENTS

We would like to thank Teruki Kamon, Nikolay Kolev and Keith Ulmer for helpful discussions. B. D. acknowledges support from U.S. Deparment of Energy (DOE) Grant No. DE-FG02-13ER42020. Y. G. acknowledges support from the Mitchell Institute for Fundamental Physics and Astronomy. D. S. acknowledges support from U.S. DOE Grant No. DEFG0292ER40701 and the Gordon and Betty Moore Foundation through Grant No. 776 to the Caltech Moore Center for Theoretical Cosmology and Physics. J. W. W. acknowledges support from the Sam Houston State University (SHSU) Enhancement Research Grant program, National Science Foundation Grant No. PHY-1521105, the SHSU Department of Physics, and the Mitchell Institute for Fundamental Physics and Astronomy.

APPENDIX A: DOUBLET DECAY IN THE SDF MODEL

Assuming $M_S < M_D$, and that the lightest $\tilde{\chi}_1^0$ is mostly the singlet S, the heavier $\tilde{\chi}_2^0, \tilde{\chi}_3^0$ are mixtures of the doublets D_1, D_2, and the squared matrix elements of their decay processes are

$$\begin{aligned}\mathcal{M}^2_{\chi_i^0\to\chi_j^0 Z} = &\frac{y^2}{2}[(M_{\chi_i^0}+M_{\chi_j^0})^2 - M_Z^2] \\ &\times[(N_{i2}N_{j1}+N_{i1}N_{j2})c_\theta + (N_{i3}N_{j1}+N_{i1}N_{j3})s_\theta]^2 \\ &+\frac{g^2+g'^2}{2}(N_{i2}N_{j2}-N_{i3}N_{j3})^2 \\ &\times(M^2_{\chi_i^0}+M^2_{\chi_j^0}+4M_{\chi_i^0}M_{\chi_j^0}-M_Z^2) \qquad \text{(A1)}\end{aligned}$$

$$\begin{aligned}\mathcal{M}^2_{\chi_i^0\to\chi_j^0 h} = &\frac{y^2}{2}[(M_{\chi_i^0}+M_{\chi_j^0})^2 - M_h^2] \\ &\times[(N_{i2}N_{j1}+N_{i1}N_{j2})c_\theta \\ &-(N_{i3}N_{j1}-N_{i1}N_{j3})s_\theta]^2, \qquad \text{(A2)}\end{aligned}$$

where s_θ, c_θ are short for $\sin\theta$, $\cos\theta$. N_{ij} are the elements of the mixing matrix that diagonalizes the mass matrix in Eq. (4). $\chi^0_{2,3}$ either decay into the singlet component of χ^0_1 via the $ySHD$ terms, or into the small doublet component in χ^0_1 via the gauge couplings.

Note that without the $ySHD$ term, i.e. in the limit $y \to 0$, the singlet would altogether decouple from the doublet, χ^0_1 would have no mixing into D_1, D_2, implying $N_{12} = N_{13} = 0$, and the prior decays would become forbidden. Turing on $y > 0$, with y still smaller than unity, the doublet mixings in χ^0_1 grow linearly with y, implying $N_{12}, N_{13} \propto y$, giving a y^2 dependence also in the second term in Eq. (A1). Thus, decay widths into both Z, h grow as y^2 when $y \ll 1$, and thereby maintain a comparable size. At large y, $y \cdot \text{vev} \sim M_S, M_D$ in the mass terms, which cause the D_1, D_2 mixings to become more complicated. Still, this property qualitatively holds, as is observed for the benchmark point III in Table III.

APPENDIX B: AEACUS EVENT SELECTION CARD

Selection cuts and computation of collider observables have been implemented within AEACUS 3.15 [14,15] using the instructions in card VI.

TABLE VI. AEACUS instruction card for computation of relevant event statistics. Prefiltering into event topology categories I–III is performed in the final lines.

1	`******** cut_card.dat v3.15 ***`
2	`* Classify Objects with No Cuts`
3	`*** Object Reconstruction ****`
4	`# ALL Jets`
5	`OBJ_JET_000=PTM:30, PRM:[ 0.0,5.0] , CUT:0`
6	`# LEAD Jet`
7	`OBJ_JET_001=SRC:+000, PRM:[ 0.0,2.5] ,`
8	`CUT:[ 1,UNDEF,-1] , OUT:PTM_001, ANY:0`
9	`# SECOND Jet`
10	`OBJ_JET_002=SRC:[ +000,-001] , PRM:[ 0.0,2.5] ,`
11	`CUT:[ 1,UNDEF,-1] , OUT:PTM_002, ANY:0`
12	`# B-Tagged Jets`
13	`OBJ_JET_003=SRC:+000, PRM:[ 0.0,2.5] , HFT:0.5, CUT:0`

(Table continued)

TABLE VI. (*Continued*)

```
14  # Non-B Jets
15  OBJ_JET_004=SRC:[ +000,-003] , PRM:[ 0.0,2.5] , CUT:0
16  # B-TAGS in Jets 1,2
17  OBJ_JET_005=SRC:[ +001,+002] , HFT:0.5, CUT:0
18  # Non-B Sub-Leading Jets
19  OBJ_JET_006=SRC:[ +000,-001,-002,-003] ,
20  PRM:[ 0.0,2.5] , CUT:0
21  # 1 B-Tags in Z/Higgs Window
22  OBJ_JET_007=SRC:+003, EFF:[ WIN,92,20,126,20,1] , CUT:0
23  # 2 B-Tags in Z/Higgs Window
24  OBJ_JET_008=SRC:+003, EFF:[ WIN,92,20,126,20,2] , CUT:0
25  # 2 B-Tags in Higgs Window
26  OBJ_JET_009=SRC:+003, EFF:[ WIN,126,20,2] , CUT:0
27  # Single Track Jets
28  OBJ_JET_010=SRC:+000, TRK:[ 1,1] , CUT:0
29  # Leading or B-Tagged Jets (No Output)
30  OBJ_JET_011=SRC:[ +001,+002,+003]
31  # Nearest B-Tag Object Pair to Higgs Window
32  OBJ_JET_012=SRC:+003, EFF:[ OIM,126,UNDEF,-1]
33  # Further B-Tag Object Pair from Higgs Window
34  OBJ_JET_013=SRC:[ +003,-012] , EFF:[ OIM,126,UNDEF,-1]
35  # ALL Leptons
36  OBJ_LEP_000=PTM:10, PRM:[ 0.0,2.5]
37  # Light Soft Leptons
38  OBJ_LEP_001=SRC:+000, EMT:-3, SDR:[ 0.3,UNDEF,1] , CUT:0
39  # Soft Taus
40  OBJ_LEP_002=SRC:+000, EMT:+3, CUT:0
41  # DiLepton Pairs in Z Window
42  OBJ_DIL_001=LEP:001, DLS:-1, DLF:1, WIN:[ 92,5] , CUT:0
43  OBJ_DIL_002=LEP:001, DLS:-1, DLF:1, WIN:[ 92,10] , CUT:0
44  ****** Event Selection *******
45  # Full Event Missing Transverse Energy
46  EVT_MET_000=OUT:1
47  # MET-Jet Delta Phi (Leading+B-Tags)
48  EVT_MDP_001=MET:000, JET:011, OUT:1
49  # MET Significance MET / sqrt( HT )
50  EVT_RHR_001=NUM:000, DEN:000, OUT:1
51  # Invariant Mass of Nearest Higgs Window Pair
52  EVT_OIM_001=JET:012, OUT:1
53  # Invariant Mass of Further Higgs Window Pair
54  EVT_OIM_002=JET:013, OUT:1
55  # Delta-R Separation of Nearest Higgs Window Pair
56  EVT_ODR_001=JET:012, OUT:1
57  # Delta-R Separation of Further Higgs Window Pair
58  EVT_ODR_002=JET:013, OUT:1
59  ****** Event Filtering *******
60  # Category I: 4 Leptons, 0+ B-Jets
61  CUT_ESC_001=KEY:LEP_001, CUT:4
62  CUT_ESC_002=KEY:JET_003, CUT:0
63  CUT_CHN_001=ESC:[ +001,+002]
64  # Category II: 2-3 Leptons, 2+ B-Jets
65  CUT_ESC_003=KEY:LEP_001, CUT:[ 2,3]
66  CUT_ESC_004=KEY:JET_003, CUT:2
67  CUT_CHN_002=ESC:[ +003,+004]
68  # Category III: 0-1 Leptons, 4+ B-Jets
69  CUT_ESC_005=KEY:LEP_001, CUT:[ 0,1]
70  CUT_ESC_006=KEY:JET_003, CUT:4
71  CUT_CHN_003=ESC:[ +005,+006]
72  ******************************
```

[1] J. R. Ellis, J. Gunion, H. E. Haber, L. Roszkowski, and F. Zwirner, Higgs bosons in a nonminimal supersymmetric model, Phys. Rev. D **39**, 844 (1989).

[2] M. Drees, Supersymmetric models with extended Higgs sector, Int. J. Mod. Phys. A **04**, 3635 (1989).

[3] L. Durand and J. L. Lopez, Upper bounds on Higgs and top quark masses in the flipped $SU(5) \times U(1)$ superstring model, Phys. Lett. B **217**, 463 (1989).

[4] C. Cheung and D. Sanford, Simplified models of mixed dark matter, J. Cosmol. Astropart. Phys. 02 (2014) 011.

[5] V. Khachatryan *et al.* (CMS), Searches for electroweak neutralino and chargino production in channels with Higgs, Z, and W bosons in pp collisions at 8 TeV, Phys. Rev. D **90**, 092007 (2014).

[6] V. Khachatryan *et al.* (CMS), Searches for electroweak production of charginos, neutralinos, and sleptons decaying to leptons and W, Z, and Higgs bosons in pp collisions at 8 TeV, Eur. Phys. J. C **C74**, 3036 (2014).

[7] D. Akerib *et al.* (LUX Collaboration), First results from the LUX dark matter experiment at the Sanford Underground Research Facility, arXiv:1310.8214.

[8] A. Djouadi, J.-L. Kneur, and G. Moultaka, SuSpect: A Fortran code for the supersymmetric and Higgs particle spectrum in the MSSM, Comput. Phys. Commun. **176**, 426 (2007).

[9] J. Alwall, M. Herquet, F. Maltoni, O. Mattelaer, and T. Stelzer, MadGraph 5: Going beyond, J. High Energy Phys. 06 (2011) 128.

[10] B. Dutta, Y. Gao, and B. Shakya, Light Higgsino decays as a probe of the NMSSM, Phys. Rev. D **91**, 035016 (2015).

[11] U. Ellwanger, C. Hugonie, and A. M. Teixeira, The next-to-minimal supersymmetric standard model, Phys. Rep. **496**, 1 (2010).

[12] T. Sjostrand, S. Mrenna, and P. Z. Skands, PYTHIA 6.4 physics and manual, J. High Energy Phys. 05 (2006) 026.

[13] J. de Favereau, C. Delaere, P. Demin, A. Giammanco, V. Lematre, A. Mertens, and M. Selvaggi (DELPHES3), DELPHES 3, A modular framework for fast simulation of a generic collider experiment, J. High Enery Phys. 02 (**2014**) 057.

[14] J. W. Walker, CutLHCO: A consumer-level tool for implementing generic collider data selection cuts in the search for new physics, arXiv:1207.3383.

[15] J. W. Walker, AEACuS 3.15, http://www.joelwalker.net/code/aeacus.tar.gz.

[16] C. Han, A. Kobakhidze, N. Liu, A. Saavedra, L. Wu, and J. M. Yang, Probing light Higgsinos in natural SUSY from monojet signals at the LHC, J. High Energy Phys. 02 (2014) 049.

[17] A. G. Delannoy, B. Dutta, A. Gurrola, W. Johns, T. Kamon *et al.*, Probing Dark Matter at the LHC Using Vector Boson Fusion Processes, Phys. Rev. Lett. **111**, 061801 (2013).

[18] G. Aad *et al.* (ATLAS), Measurements of Four-Lepton Production at the Z Resonance in pp Collisions at $\sqrt{s} = 7$ and 8 TeV with ATLAS, Phys. Rev. Lett. **112**, 231806 (2014).

[19] G. Aad *et al.* (ATLAS Collaboration), Search for squarks and gluinos with the ATLAS detector using final states with jets and missing transverse momentum and 4.7 fb^{-1} of $\sqrt{s} = 7$ TeV proton-proton collision data, ATLAS-CONF-2012-033; Phys. Rev. D **87**, XML012008 (2013).

[20] Search for Supersymmetry in hadronic Final states using M_{T2} with the CMS detector at $\sqrt{s} = 7$ TeV, Report No. CMS PAS SUS-12-002.

[21] C. Lester and D. Summers, Measuring masses of semiinvisibly decaying particles pair produced at hadron colliders, Phys. Lett. B **463**, 99 (1999).

[22] Y. Bai, H.-C. Cheng, J. Gallicchio, and J. Gu, Stop the top background of the stop search, J. High Energy Phys. 07 (2012) 110.

[23] S. Chatrchyan *et al.* (CMS Collaboration), Search for physics beyond the standard model in events with a Z boson, jets, and missing transverse energy in pp collisions at $\sqrt{s} = 7$ TeV, Phys. Lett. B **716**, 260 (2012).

[24] S. Chatrchyan *et al.* (CMS Collaboration), Inclusive search for squarks and gluinos in pp collisions at $\sqrt{s} = 7$ TeV, Phys. Rev. D **85**, 012004 (2012).

[25] C. Rogan, Kinematical variables towards new dynamics at the LHC, arXiv:1006.2727.

[26] CMS Collaboration, SUSY searches with dijet events, Report No. CMS PAS SUS-08-005.

[27] L. Randall and D. Tucker-Smith, Dijet Searches for Supersymmetry at the LHC, Phys. Rev. Lett. **101**, 221803 (2008).

[28] CMS Collaboration, Search strategy for exclusive multi-jet events from supersymmetry at CMS, Report No. CMS PAS SUS-09-001, http://cdsweb.cern.ch/record/1194509.

[29] S. Chatrchyan *et al.* (CMS Collaboration), Measurement of the Polarization of W Bosons with Large Transverse Momenta in W + Jets Events at the LHC, Phys. Rev. Lett. **107**, 021802 (2011).

[30] CMS Collaboration, Search for supersymmetry in pp collisions at $\sqrt{s} = 7$ TeV in events with a single lepton, jets, and missing transverse momentum, Report No. CMS PAS SUS-11-015.

[31] G. Aad *et al.* (ATLAS Collaboration), Measurement of event shapes at large momentum transfer with the ATLAS detector in pp collisions at $\sqrt{s} = 7$ TeV, Eur. Phys. J. C **72**, 2211 (2012).

[32] V. Khachatryan *et al.* (CMS Collaboration), First measurement of hadronic event shapes in pp collisions at $\sqrt{(s)} = 7$ TeV, Phys. Lett. B **699**, 48 (2011).

[33] A. Banfi, G. P. Salam, and G. Zanderighi, Resummed event shapes at hadron-hadron colliders, J. High Energy Phys. 08 (2004) 062.

[34] M. Guchait and D. Sengupta, Searches for supersymmetry at the LHC with 7 TeV energy, Phys. Rev. D **84**, 055010 (2011).